Review



# Thermal Effects on Optical Chirality and Associated Symmetry Properties

Hyoung-In Lee * , Tanvi Vaidya , Ram Prakash Dwivedi

Posted Date: 20 February 2023

doi: 10.20944/preprints202302.0328.v1

Keywords: chirality; helical conformation; constitutive relations; temperature-dependent; magnetoelectric coupling; light-matter interaction; meta-atom; thermal helical inversion; enantiomeric excess; chiral switching

*Review*

# Thermal Effects on Optical Chirality and Associated Symmetry Properties

**Hyoung-In Lee [1,*], Tanvi Vaidya [2] and Ram Prakash Dwivedi [3]**

[1] Research Institute of Mathematics, Seoul National University, 599 Gwanak-Ro, Gwanak-Gu, Seoul 08826, Republic of Korea
[2] School of Electrical and Computer Science Engineering, Shoolini University, Himachal Predesh, India; tanvi.vaidya7@gmail.com
[3] School of Electrical and Computer Science Engineering, Shoolini University, Himachal Predesh, India; rpdwivedi@shooliniuniversity.com
* Correspondence: hileesam@naver.com

**Abstract:** A review is here provided on the thermal effects on the optical chirality. To this goal, chiral objects dispersed in an embedding fluid are examined for their magnetoelectric coupling. Archetypal twisted-Omega particles are examined with respect to electron transport, phonon dynamics, and temperature effects. Continuum-mechanical aspect of thermo-elasticity is reviewed along with transverse deformations. A transition temperature delineating a sign flip in the chirality parameter is identified as well.

**Keywords:** chirality; helical conformation; constitutive relations; temperature-dependent; magnetoelectric coupling; light-matter interaction; meta-atom; thermal helical inversion; enantiomeric excess; chiral switching

## 1. Introduction

Conventionally, 'chiral' is a geometric notion indicating 'non-mirror symmetric' [1]. For this reason, 'helical' refers to 'geometry (conformation)' in this study, while 'chiral' is associated with '(optical) property'. Sometimes, 'chirality' stands for a mere 'geometric chirality' without any associated phenomena [2,3]. Nature provides us with ample examples of chirality in the fields of biology, chemistry, and minerals [4].

Consider field-matter interactions illustrated on Figure 1. Notice henceforth that jargons for continuum mechanics and those for quantum mechanics are mixed up without too much rigor. For the sake of our study, the fields (in the outer rectangular domain on Figure 1) are classified into temperature field, acoustic field (stress field or phonons), electric field, magnetic field, and electromagnetic (EM) field. Meanwhile, matters (in the inner rectangular domain in Figure 1) are grouped into dielectric (non-electric and non-magnetic), electric matter, magnetic matter, magnetoelectric (ME) matter. Sharp delineations of fields and matters presented on Figure 1 are made just for convenience since they may cause controversy from rigorous viewpoints.

Consider elasticity (phonon dynamics) indicated by (a) on Figure 1, where interactions between phonons within matters and acoustic (stress) field take place. The temperature dependence shows itself up through the Bose factor of the form involving $\exp(\hbar\omega/k_B T)$. Here, $\{\hbar, \omega, k_B, T\}$ are the reduced Planck constant, frequency, the Boltzmann constant, and temperature, respectively. Thermo-acoustic effects are marked by (b) on Figure 1, of which temperature-dependent refractive indices make one example [5].

The item 'dielectrics' listed as one of 'matters' on Figure 1 refer to non-electric and non-magnetic media in this study. Dielectrics include, say, vacuum, air (approximately), and normal glasses. Electric matters refer here, say, to non-magnetic metals such as gold, silver, and copper. Consider the situation with the Landau quantization as marked by (c) on Figure 1, where applied electric and

Preprints (www.preprints.org) | NOT PEER-REVIEWED | Posted: 20 February 2023 doi:10.20944/preprints202302.0328.v1



magnetic fields influence an electrically conducting strip. A transverse electric current is established from interactions between magnetic field and electric matter. Normally, thermal effects are not considered for the Landau quantization.

Temperature effects are considered in the context of a chiral spin Seebeck effect [6] (pp. 1-23), [7]. As illustrated by (d) on Figure 1, couplings among two Kittel modes and one film magnon are examined in [6] (pp. 1-23). Mechanical deformations (phonons) and attendant thermal effects have been taken into consideration for magnetic materials [8,9] and other matters [10]. As illustrated as interactions among electromagnetic field, electric matter, and dielectric by (e) on Figure 1, surface plasmon waves are established between a metal and a dielectric medium. Optical losses would then lead to thermal effects that might influence in turn the metals' optical performance.

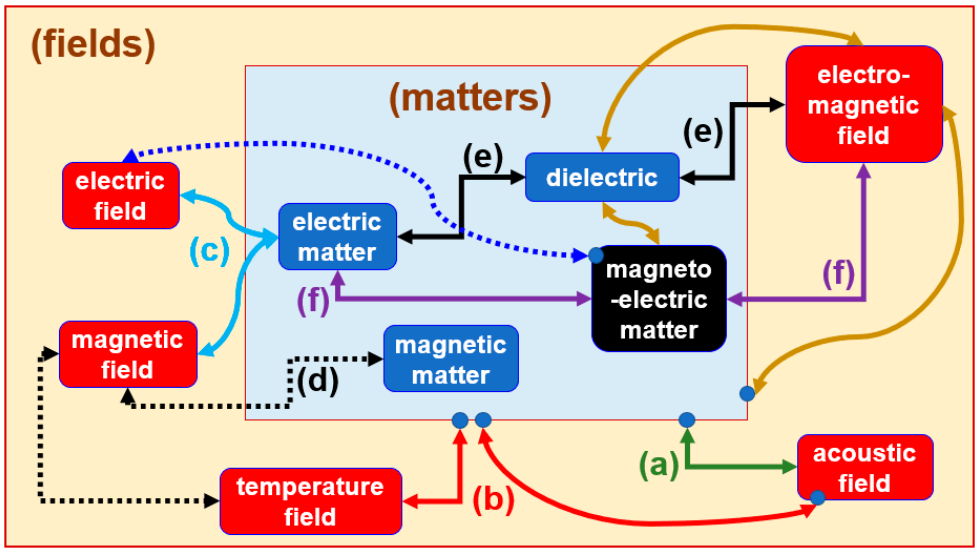


**Figure 1.** Field-matter interactions. (a) elasticity (acoustic field, matter), (b) thermo-elasticity (thermal field, acoustic field, matter), (c) electron dynamics of Landau quantization (electric field, magnetic field, electric matter), (d) electron dynamics of spin waves (thermal field, magnetic field, magnetic matter), (e) achiral surface plasmon waves (electromagnetic field, electric matter, dielectric), (f) chiral surface plasmon waves (electromagnetic field, magnetoelectric matter, electric matter). Semiconductors as matters cannot be easily fit into the above picture.

The purpose of this study is to identify the thermal effects on chiral media. To this goal, we will focus on helical structures, for which thermal effects will be further discussed. Both chiral molecules dispersed in fluids and artificial chiral meta-atoms imbedded in solids are affected by variations in temperature. Key idea of this article is to examine how temperature variations cause structural changes in the chiral molecules and artificial chiral meta-atoms. To this goal, relationships among phonons, electrons, and thermal fields will be examined in connection with temperature variations.

This study is hence structured in the following way. Section 2 briefly examines the electric, magnetic, and magnetoelectric matters for which constitutive relations are discussed for the Maxwell equations. Section 3 largely handles mechanical deformations of chiral objects. In this connection, a twisted Ogema particle is introduced as an archetypal magnetoelectric matter. Section 4 takes flat fishes as an example to show various aspects of chirality. Section 5 treats thermal effects of chiral objects in connection to phonons and electrons. Section 6 offers discussion on how chiral objects get into interaction with embedding fluids. Section 7 concludes our review.

## 2. Chiral Media and Constitutive Relations

Having briefly touched upon electric matter and magnetic matter in the preceding section, magnetoelectric (ME) matter is supposed to contain both features of electric matter and magnetic

Preprints (www.preprints.org) | NOT PEER-REVIEWED | Posted: 20 February 2023 doi:10.20944/preprints202302.0328.v1



matter. Field-matter interactions are then reduced to light-matter interactions when EM fields are considered instead of separated electric field and magnetic field.

Consider a twisted Omega particle (meta-atom) made of a conducting material as depicted on Figure 2a, for which Figure 2 of [11] is more illustrative. This meta-atom consists of a single circular loop with a cut at the two ends of which two finite-length cylindrical wires are attached in the direction perpendicular to the plane of a circular loop [11,12].

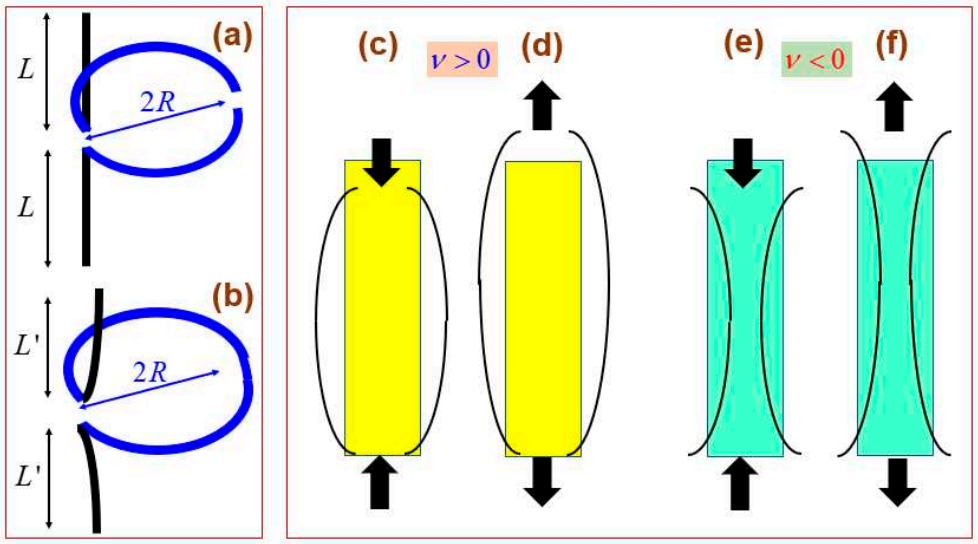


**Figure 2.** (a) A three-dimensional twisted Omega particle. Two straight wire portions are of finite length $L$ and of radius $a$, whereas the looped portion is of radius $R$. The plane of the looped portion is perpendicular to the straight wire portions. (b) An exaggerated view of a twisted Omega particle after a thermal expansion, whereby the radius of the looped portion is made larger than that shown on (a). Schematics for a circular column under (c,e) compression and (d,f) stretching in the axial direction. (c,d) for a positive Poisson ratio with $\nu > 0$, (e,f) for a negative Poisson ratio with $\nu < 0$.

Suppose that a plane EM wave incident onto such a twisted Omega particle, where the electric field is assumed to be established parallel to the straight wire portions. In the meantime, induced currents are then established along the whole twisted Omega particle from a simple viewpoint. In turn, an effective magnetic field is induced in the direction parallel to the straight portion due to the induced electric current along the looped portion [13]. Consequently, a twisted Omega particle carries intrinsically the magnetoelectric (ME) coupling [11,14,15].

Wire-loop geometry can be modified by introducing a certain degree of asymmetry. To this end, consider a unit cell of 'U-shaped loop by two T-shaped strips ('U-shaped loop' for short') presented on Figures 2 and 3 of [16]. This U-shaped loop is made of conducting and non-gyrotropic material. Due to its geometric symmetry, this U-shaped loop is mirror-symmetric (thus being achiral). However, an electric transistor is loaded onto one arm of the U-shaped loop portion.

Resultantly, an electric loop current along the U-shaped loop portion is prohibited from flowing in a certain direction, leaving an electric loop current only in one direction along the U-shaped loop portion. The resulting nonreciprocity or unidirectional electric current in [16] is thereby established. Therefore, a meta-surface can be built up by an array consisting of such 'transistor-loaded' U-shaped loops. This nonreciprocity effectively gives rise to EM chirality owing to the non-antisymmetric transistor. Although this idea is worthwhile, it remains to further miniaturize the unit cell such that it works with higher frequencies. The addition of an electric transistor also demands extra fabrication cost as well.

As biological materials, double-helix (double-strand) DNAs (deoxyribo nucleic acids) are the most notable twisted structure [17]. The geometry of a DNA is characterized by a pair of parameters: the diameter and the pitch of a helix [18,19]. The electron transport within a DNA-like structure is

Preprints (www.preprints.org) | NOT PEER-REVIEWED | Posted: 20 February 2023 doi:10.20944/preprints202302.0328.v1



found to be strongly dependent on this pair of parameters [20–22]. A typical problem of electron transport in chiral objects is that of along a helix. In this respect, consider the chirality-induced spin selection (CISS) [20,21,23–25], whereby electron spins of particular spin directions are preferentially selected according to the chirality of the geometric device. This CISS is also found to strongly depend on temperature as in many magnetic phenomena. In a similar line of reasoning, a chirality-controlled (selective) synthesis (CCS) offers us a challenge in fabricating carbon nanotubes of a certain desired handedness [3].

Suppose that a liquid is uniformly dispersed by an ensemble of twisted Omega particles. This homogeneous mixture makes an example of what we call a 'chiral medium'. An embedding (surrounding) medium is alternatively called a solvent. In general, a mean-field theory holds true more accurately for sparsely dispersed chiral media than densely dispersed ones [13,26].

As marked by (f) on Figure 1, surface plasmon waves are established between a metal and a chiral medium [15,27,28], for which the term chiral surface plasmon resonance (CHISPR) is coined in [6] (pp. 25-52). The CHISPR stands for interactions among electromagnetic field, magnetoelectric matter (a chiral medium), and electric matter (a metal). Both geometric configuration and stereochemical structures of chiral objects determines their response to applied fields [29] (pp. 97-116), [30,31]. Chiral media containing magnetic chiral objects could also lead to plasmonic resonances [6] (pp. 53-74), [32].

Chirality is a geometric notion equivalent to mirror asymmetry, which is associated with two additional features [13,33]. Firstly, chirality is manifests itself through a rotation of the polarization plane of EM waves propagating through a chiral medium. The polarization rotation is alternatively termed 'optical rotatory dispersion (ORD)' [2,6,34–36]. Secondly, chirality is largely accompanied by magnetoelectric (ME) coupling [6,11,14,35,37]. Both ORD and ME coupling are associated with spin-orbit coupling (SOC) [14,20,23,38,39]. Of course, both ORD and ME coupling could be established by means other than chiral media. As an example, magnetic achiral media could induce ORD as seen with Faraday rotation [38].

**Table 1.** Two types of embedding media with comparative characters. The dispersed chiral objects (building blocks) may be either natural (DNAs, sugar, human bodies, etc.) or man-made (artificial) meta-atoms (screws, twisted Omega particles, Moebius strips, gloves, wire braids, wire helices, etc.).

| embedding media | fluids or soft matters | solids or condensed matters |
|---|---|---|
| comparative features | randomly oriented, position-independent, strongly temperature-dependent | periodically and regularly oriented, position-dependent, weakly temperature-dependent |
| references | [11,15,18,20,21,24,29,30,40,41]. | [6] (pp. 75-103), [12,13,19,26,36,42]. |

Chiral media are enjoying renewed interests in optics. The reason lies in the availability of chiral objects obtainable by various nanofabrication techniques [2,15,43]. In many instances, chiral metamaterials are solid media periodically imbedded with chiral objects of artificial meta-atoms. Table 1 provides a summary of two types of chiral media: [i] chiral media, where a fluid is uniformly dispersed by an ensemble of chiral objects, and [ii] chiral meta-materials. We are focusing on the chiral media in this study, although there are far more research activities and fabrication techniques developed for chiral meta-materials.

The '*electromagnetic (EM) chirality*' is constructed from both $\mathbf{E}\bullet\nabla\times\mathbf{E}$ and $\mathbf{H}\bullet\nabla\times\mathbf{H}$, where $\{\mathbf{E},\mathbf{H}\}$ are electric and magnetic field vectors [6] (pp. 75-103), [13,44]. Oftentimes, 'EM chirality' is alternatively and confusingly called a 'light helicity' [15]. For the forthcoming symbols, we employ the overbar '-' for dimensional variables and parameters. In comparison, symbols without the overbar '-' are dimensionless. Consider the following set of Maxwell equations with the usual meanings for the participating variables and parameters.

Preprints (www.preprints.org) | NOT PEER-REVIEWED | Posted: 20 February 2023 doi:10.20944/preprints202302.0328.v1



$$\begin{cases} \nabla\times\mathbf{E}=\mathrm{i}\omega\mathbf{B} \\ \nabla\times\mathbf{H}=-\mathrm{i}\omega\mathbf{D} \end{cases}, \quad \begin{cases} \nabla\bullet\mathbf{D}=0 \\ \nabla\bullet\mathbf{B}=0 \end{cases} \tag{1}$$

Here, $\{\mathbf{D},\mathbf{B}\}$ are electric displacement and magnetic flux density. These equations take dimensionless forms, for which the scheme of making various variables and parameters is detailed in [45].

In addition, either of the following pairs of constitutive relations (CRs) is employed.

$$CR_\kappa:\begin{cases} \mathbf{D}=\varepsilon\mathbf{E}+(\chi+\mathrm{i}\kappa)\mathbf{H} \\ \mathbf{B}=\mu\mathbf{H}+(\chi-\mathrm{i}\kappa)\mathbf{E} \end{cases};\quad CR_\beta:\begin{cases} \mathbf{D}=\varepsilon(\mathbf{E}+\beta\nabla\times\mathbf{E}) \\ \mathbf{B}=\mu(\mathbf{H}+\beta\nabla\times\mathbf{H}) \end{cases}. \tag{2}$$

Here, $\{\varepsilon,\mu\}$ are the dimensionless electric permittivity and magnetic permeability, respectively. The dimensional chirality parameters $\{\bar{\kappa},\bar{\beta}\}$ are related to the dimensionless chirality parameters $\{\kappa,\beta\}$ through the respective relations $\kappa\equiv\bar{c}_0\bar{\kappa}$ and $\beta\equiv\bar{k}_0\bar{\beta}$. Furthermore, $\bar{c}_0$ is the light speed in vacuum and $\bar{k}_0\equiv\bar{\omega}_0/\bar{c}_0$, where $\bar{\omega}_0$ is a certain prescribed frequency. The Tellegen parameter $\chi$ represents material loss of chiral objects [19,46]. In case with $\chi\neq 0$, we can easily come up with the circular dichroism (CD) with differential absorptions [13,15,19]. We will henceforth set $\chi=0$ for simplicity so that both of $\{\kappa,\beta\}$ are assumed real.

This pair of CRs are valid for chiral media with various dispersed building blocks (both natural chiral objects and artificial chiral meta-atoms). In case with fluids randomly dispersed with chiral objects, both of $\{\kappa,\beta\}$ are roughly proportional to the relative volume of the immersed chiral objects [11]. Besides, $\kappa$ is alternatively dubbed a 'chiral admittance' [31], while it is proportional to the anisotropy factor [35]. By effective medium theory [47], angular averaging is taken for orientationally ordered chiral objects [15,35,48]. For metamaterials that contain positionally ordered meta-atoms, such an isotropy would not hold true.

Quantum-mechanical formulas for $\kappa$ are constructed based on oscillator models with linear perturbations [35]. In this respect, the Born-Kuhn model for coupled oscillators is employed for the analysis of interparticle EM interactions [2,8].

**Table 2.** Two types of constitutive relations for chiral media and comparative characters.

| types of constitutive relations | Pasteur constitutive relations | Drude-Born-Fedorov (DBF) constitutive relations |
|---|---|---|
| formulas | $CR_\kappa:\begin{cases}\mathbf{D}=\varepsilon\mathbf{E}+\mathrm{i}\kappa\mathbf{H}\\ \mathbf{B}=\mu\mathbf{H}-\mathrm{i}\kappa\mathbf{E}\end{cases}$ | $CR_\beta:\begin{cases}\mathbf{D}=\varepsilon(\mathbf{E}+\beta\nabla\times\mathbf{E})\\ \mathbf{B}=\mu(\mathbf{H}+\beta\nabla\times\mathbf{H})\end{cases}$ |
| Comparative features | field variables only, more commonly employed, only local terms | Both field variables and their spatial gradients, less commonly employed, both local and nonlocal terms |
| references | [6] (pp. 25-52), [11,13,19,27,30,35–37,44,49]. | [13,31,48,50] |
| | [31,51]. | |

The first pair $CR_\kappa$ is called the 'Pasteur' CRs, whereas the second pair $CR_\beta$ is called the 'Drude-Born-Fedorov (DBF)' CRs. Both $\{CR_\kappa,CR_\beta\}$ refer to bi-isotropic chiral media respectively with single chirality parameters $\{\kappa,\beta\}$. To the leading order in small values of $\{\kappa,\beta\}$, namely, for $|\kappa|,|\beta|\ll 1$, both of $\{CR_\kappa,CR_\beta\}$ are approximately equivalent [30]. In general, the Pasteur CRs are more acceptable. Comparative features of $\{CR_\kappa,CR_\beta\}$ are summarized in Table 2 together with pertinent references.

Preprints (www.preprints.org) | NOT PEER-REVIEWED | Posted: 20 February 2023 doi:10.20944/preprints202302.0328.v1



CRs are alternatively called the 'material connections (MCs)' [35]. Moreover, optically active liquids (say, octyl alcohol, limonene, ethyl tartrate, etc.) consisting homogeneously of chiral molecules are investigated to show the dependence of $\kappa$ on several parameter: the density of liquid, the number densities of chiral constituent molecules, electric and magnetic polarizabilities of molecules, quantum-transition probabilities, etc. [35]. In addition, a more sophisticated pair of CRs is presented in [35] such that it adds transient (time-dependent) terms to the instantaneous forms given in Equation (2) [48].

Chiral media carry bi-isotropic responses to EM fields, where the effective refractive indices are given respectively as follow [29,35,50,51].

$$CR_\kappa : \sqrt{\varepsilon\mu} \pm \kappa; \quad CR_\beta : \frac{\sqrt{\varepsilon\mu}}{1 \mp \sqrt{\varepsilon\mu}\omega\beta}. \tag{3}$$

Of course, we obtain the effective refractive index $\sqrt{\varepsilon\mu}$ for achiral cases with $\kappa, \beta = 0$. For larger chirality parameter with $\sqrt{\varepsilon\mu} < |\kappa|$ or $1 < \sqrt{\varepsilon\mu}\omega|\beta|$, negative refractive index could be obtained [13,19,29,43]. An extended version of $CR_\beta$ is presented in the name of spatial-spectral CRs by [13]. In addition, both of $\{\kappa, \beta\}$ are frequency-dispersive in general [2,15,34–36].

The Pasteur CRs $CR_\kappa$ carry only local terms involving $\{\mathbf{E}, \mathbf{H}\}$. In comparison, nonlocal portions $\{\varepsilon\beta\nabla\times\mathbf{E}, \mu\beta\nabla\times\mathbf{H}\}$ with spatial derivatives are seen in $CR_\beta$ [13,48]. Hence, $CR_\kappa$ lends itself to simpler interpretation than $CR_\beta$. Moreover, a pseudoscalar property of $\kappa$ is evident, whereas pseudoscalar property of $\beta$ is less clear [35,52] (p. 243).

The controversy as to whether constitutive relations (CRs) contain spatial derivatives or not is also encountered in fluid dynamics. For instance, Korteweg-type CRs include not only standard fluid-dynamic variables but also the density gradient in the context of Korteweg tensor [53,54]. Instead of the local Newtonian stresses, capillary forces in fluids are more adequately accounted for by the Korteweg stresses, whence the temperature dependence of capillarity is accounted for. In this respect, the Korteweg-type CRs are based on an extended version of nonequilibrium thermodynamics. Those Korteweg-like CRs are derived using the second gradient theory [55], where the concepts like multipolarity or interstitial dynamics have been resorted to.

Notice that capillary flows invariably involve non-planar spatial domains, from which we expect complicated geometrical configurations of chiral embedded objects to be better represented by the curl-based $CR_\beta$. Both flows of compressible fluids discussed in [53,54] and the EM waves propagating through chiral media are accompanied by bi-characteristics provided by Equation (3). It remains for us to see whether the curl-based constitutive relations $CR_\beta$ better describe the multipolar electrodynamics and the magnetoelectric (ME) coupling hidden under the light-matter interactions occurring through chiral media [35].

In concrete examples for the propagations of EM waves through chiral media with appropriate boundary conditions, it is found that most of problems are solved with $CR_\kappa$, while a few exceptional problems are solved with $CR_\beta$ as listed in Table 2. Therefore, we are focusing oftentimes on $CR_\kappa$ in this study for convenience.

A usefulness of chirality parameter $\kappa$ can be seen by supposing a liquid that is homogeneously dispersed by a random ensemble of chiral molecules. In this case, the rotation angle $\theta_{ORD}$ of the polarization plane of EM waves propagating through a distance $\bar{d}$ is given by the following [6] (pp. 25-52), [18,35].

$$\theta_{ORD} = 2\frac{\bar{d}\,\bar{\omega}}{\bar{c}_0}\kappa \tag{4}$$

Here, the subscript 'ORD' stands for the afore-mentioned 'optical rotatory dispersion (ORD)'. The optical rotation (OR) angle also refers to Equation (4) [33].

 doi:10.20944/preprints202302.0328.v1



The induced electric currents within a twisted Omega particle can be handled with a simplest single-electron model of Condon [19,35], where the geometric helical paths occupied by helical nanostructures are replaced by chiral confining potentials [20,21,35]. Unfortunately, only the frequency dependence $\kappa(\omega)$ is reported by [19], thus leaving us with another difficult task of finding geometric dependence $\kappa(geometry)$ of helical nanostructures. For large chirality parameters, nonlinear analyses might be necessary [48].

### 3. Mechanical Properties of Chiral Objects

Figure 2b depicts an exaggerated view of a deformed configuration for a twisted Omega particle shown on Figure 2a. Suppose that either mechanical forces due to neighboring structures or thermal effects cause such deformations. Consider a cylindrical column of finite length as depicted on Figure 2c–f. The Poisson ratio $\nu$ written on Figure 2c–f is defined to be the negative of a lateral (radial) strain to a longitudinal (axial) strain [6] (pp. 287-322), [56,57].

Under mechanical excitations, the two straight portions on Figure 2a would experience either compression or stretching as depicted on Figure 2c,d. In comparison, the looped portion on Figure 2a may experience a combination of compression and stretching depending on the geometric relationship between the loop plane and a mechanical excitation. Consequently, the chirality parameter varies with the Poisson ratio, namely, $\kappa(\nu)$ and $\beta(\nu)$.

Both Figure 2c,d are obtained in case of the Poisson ratio being positive, viz., $\nu > 0$. Consider Figure 2c firstly. Under compression in the axial longitudinal direction, the lateral diameter is enlarged in compensation for the axial shortening. Consider Figure 2d secondly. Under decompression in the axial longitudinal direction, the lateral diameter is shortened in compensation for the axial elongation (or prolongation) [3]. As depicted on Figure 2e,f, opposite changes in the length and diameter take place for the Poisson ratio being negative, viz., $\nu < 0$.

By the volume conservation of a homogeneous material, it is required for isotropic linear elastic materials that $-1 < \nu < \frac{1}{2}$ for three-dimensional structures and $-1 < \nu < 1$ for two-dimensional structures [58,59]. Soft matters such as DNAs are endowed with larger values of $\nu$, while hard matters such as concretes are equipped with smaller values of $\nu$. Meanwhile, the Poisson ratios of metals are relatively large. For instance, $\nu \approx 0.33$ for copper and $\nu \approx 0.43$ for gold.

Periodic structures could however exhibit effective negative Poisson ratios such as seen with two-dimensional chiral honeycombs [60,61]. Depending on specific materials, negative Poisson ratios may lead to unexpected chirality parameters. Referring Figure 2e,f, it will be extremely interesting to examine the EM chirality of a twisted-Omega-like particle made of auxetic media with negative Poisson ratio, namely, $\nu < 0$.

It is reported in [58] that $-14 < \nu < 0$ for an anisotropic polytetrafluoroethylene (PTFE) in a true strain range of 0.03. From viewpoints of stereochemistry, this anisotropic PTFE consists of chains of atoms and bonding members. For continuous solids, the apparent Poisson ratio is proportional to the atomic packing density (APD) of the constituent molecules for crystalline metals. From a simple reasoning, the higher the APD the harder a given material becomes. Harder materials resist a lateral deformation for a given longitudinal deformation. Therefore, the Poisson ratio becomes smaller with increasing APD.

In case with a metamaterial consisting of periodically folded sheets (say, Origami), an effective Poisson ratio ranging over $-5 < \nu < 5$ is reported [62]. In such mechanical metamaterials, the effective Poisson ratio is varied depending on the direction of applied force. Mechanical deformations such as buckling should be taken into consideration during and after fabrications of twisted-Omega-like chiral objects and other helical structures [6] (pp. 241-263). In the case of subwavelength small nanoparticles (NPs), the surface plasmon resonance can be gradually tuned via prolongation of the NP along one axis covering the whole visible and near-infrared (IR) region [10]. In this aspect, magnetoelastic waves are analyzed in [6] (pp. 287-322).

Let us examine basic dynamical modes of a thin tube made of a single elastic material [63]. Suppose that deformations in linear elasticity follow $\exp(im\theta + iz)$, where $\{\rho, \theta, z\}$ are cylindrical

Preprints (www.preprints.org) | NOT PEER-REVIEWED | Posted: 20 February 2023 doi:10.20944/preprints202302.0328.v1



coordinates. Figure 16 of [63] illustrates three lowest dynamic vibrational modes: a radial breathing mode (RBM) for $m=0$, a helix mode (RBM) for $m=1$, and an ovalization mode for $m=2$. Therefore, nonzero chirality is established for $m>1$. Since boundary conditions could select which modes to prevail with time, it is important to design a whole elastic system for achieving a desired dynamic chirality. The 'achiral' RBM plays a key role in the near-field Raman spectroscopy in extracting structural information on the chiral carbon nanotubes [64].

In case with a twisted Omega particle shown on Figure 2a [11], a helix with longer wire portions could be gradually shortened into a helix with shorter wire portions. Instead, the radius of the loop portion of that helix gets increased with a resultant shorter pitch. This decreased pitch is achieved under the action of forces produced by the induced electric currents along the helix. The forces induced by the currents along a helix is supposed to be caused by Coulomb repulsion, although Coulomb force may be incompatible with material chirality [52] (p. 208). Roughly speaking, the helix under induced currents gets less chiral from the viewpoint of EM waves. Conversely, a helix with shorter wire portions would lead to larger chirality. According to a naïve idea, increased temperature would reduce the geometric helicity of twisted Omega particles, thereby reducing their optical chirality.

What about twisted Omega particles made of non-metallic materials? An answer to this self-raised question is obtained by examining optics for all-dielectric systems. An all-dielectric system here refers to, say, a dielectric structure sitting on a dielectric substrate [12], both being laid down in vacuum. Simply put, even all-dielectric systems could exhibit both electric and magnetic multipoles [52] (pp. 217-242), if illuminated by non-simple EM fields. This fact was demonstrated by the Mie scattering off a dielectric sphere immersed in an embedding dielectric medium [65]. The way this all-dielectric optical system gives rise to a ME coupling is by means of the interference between an incident field and a scattered field [65].

All-dielectric systems come with low losses compared to plasmonic systems so that dielectric chiral meta-surfaces are actively pursued in recent years. These benefits made possible by all-dielectric systems demand instead dielectric materials of higher refractive indices, say, niobium pentoxides [6] (pp. 91-93) or electro-optic (EO) materials such as vanadium dioxides [66]. In this connection, we need data for not only heat capacity but also enthalpy of formation and Gibbs energy [67], which are necessary for accounting for conformational changes.

Consider a waveguide made of silicon oxynitride [5], where an effective refractive index $n_{eff}$ can be evaluated [29]. The resulting thermo-optic coefficient $dn_{eff}/dT$ obtained from the setting of a waveguide shows a strong temperature dependence. It remains to verify the easy manufacturability of dielectric materials into twisted Omega particles presented on Figure 2a. During fabrication, an additional issue of residual stresses should be taken care of. An analogous effect plays a key role in realizing thermally induced refractive-index gratings in Yb-doped fibers [68]. It remains to be seen how to implement such thermo-optic effects in constructing helix-like structures with analogous controllability.

A dielectric elastomer is actuated by applied electric potential so that even a necking phenomenon might take place based on a positive Poisson ratio as illustrated on Figure 1 of [69]. Through careful fabrication, a multilayer stack of helical shape can also be realized as depicted on Figure 11 of [69] and on various figures of [70]. Such stacked configurations offer easier contractibility along its longitudinal axis. Furthermore, helical stacked multilayer configurations provide us with electrically contractile monolithic actuators when alternating flexible electrodes are interposed [70]. It remains to be seen how to further miniaturize those electroactive polymers (EAPs) employed in [70] for the purpose of being employed as EM meta-atoms.

Electron-phonon dynamics (elasticity in continuum mechanics) is largely inseparable from thermal effects. Considering the electron dynamics along DNA-like helical structures [21], temperature-dependent electron dynamics is envisaged if electron-phonon interactions come additionally into play [10]. Notwithstanding, such required electron-phonon interactions should be of appropriate form for nonzero chirality parameter to be established [35], which can be seen also from the molecular-dynamics simulation results [3,71].

Preprints (www.preprints.org) | NOT PEER-REVIEWED | Posted: 20 February 2023 doi:10.20944/preprints202302.0328.v1



When a droplet of chiral liquid crystal (LC) is immersed in an achiral isotropic liquid, rotational and helical motions due to local deformations can be identified within a finite-sized chiral LC droplet [1,72]. Notice here that rotational motions are related to shear stresses [29] (pp. 97-116).

Vibrational motions of atom-bonding chains can be categorized into rotational and longitudinal ones along the axis of a bridging bond as viewed from stereochemistry. The retrieval of such different vibrational modes is required in properly interpreting the Raman scattering data obtained on the frequency spectral domain [6] (pp. 53-74), [37]. Recall that the Raman spectroscopy involves interactions among electrons, phonons, and photons. The temperature dependence (through the Bose factor) of Raman spectra is indicative of the temperature dependence of various vibrational modes of phonons [73]. In case with helix-shaped structures, it is necessary in general to infer from the Raman signals the desired structural information such as pitches and radii [2,10]. Such data extraction constitutes inverse problems from a mathematical point of view.

## 4. Chirality of Flat Fishes

Mechanical effects are sometimes accompanied by energetic effects and reactivity [4]. In this connection, recall the famous Korean phrase cited by Korean fishermen: 'left-Gwang-right-Do' [74]. Here, 'Gwang' refers to the fish 'Gwang-Uh' in Korean, which refers in turn to 'Paralichthyidea olivaceus' in official terms (being called just 'olivaceus' here for simplicity). In the meantime, 'Do' refers to the fish 'Do-Da-Rie' in Korean, which refers in turn to 'Pleuronichthys cornutus' in official terms (being called just 'cornutus' here for simplicity). Therefore, let us rephrase 'left-Gwang-right-Do' into 'left-olivaceus-right-cornutus (LORC)' from now on.

Simply put, these flat fishes are two-dimensional (2D) enantiomers in sizes on the order of 15 centimeters by 25 centimeters. In comparison, their thickness is about 4 centimeters. Arrays of those fishes could be dried on flat panels or roofs (viz., meta-surfaces) for later storage. Meanwhile, EM waves of wavelengths on the order of 1 meter (radio waves) or longer could recognize 2D arrays of those fishes as chiral meta-surfaces.

With Figure 3, let us examine the details of either mirror-symmetry or mirror-asymmetry for these flat fishes. Figure 3a illustrates a baby fish swimming freely in seawater. As it grows up within a year or so after it was hatched from an egg, its genetic codes advise it to stay on the sandy bottom of a sea, normally located about a couple of 100 meters deep. So begins its life near the bottom of a sea. Sometimes it flips itself or swims. Other times, it tries to catch other smaller fishes by moving itself elsewhere. However, it spends most of its time on the bottom of sea. Hence, its body becomes flatter with time as illustrated on Figure 3b. It still has a finite thickness, but it becomes almost-2D-like within a year or so. Such a flattening compression process due to hydrostatic pressure in deeper sea might have taken with $\nu > 0$ as depicted on Figure 2c, with a growing process superimposed.

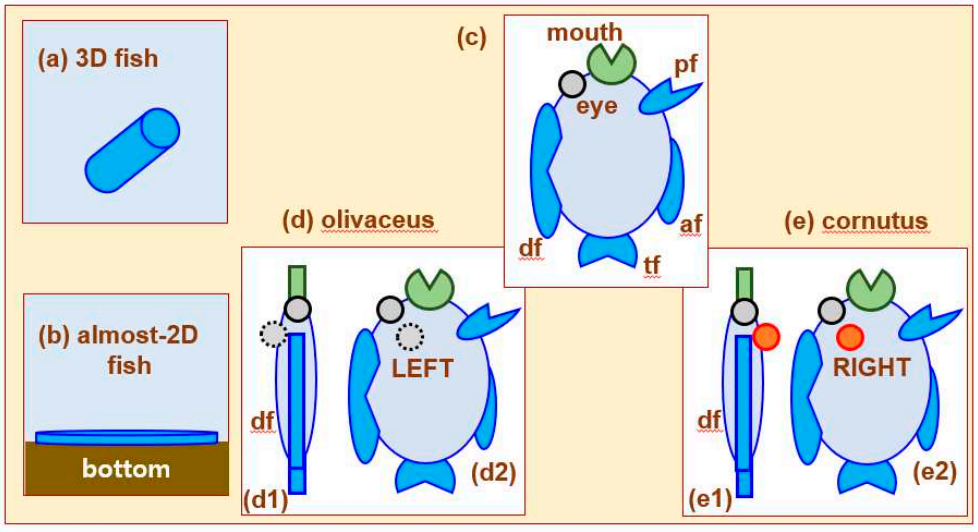

 doi:10.20944/preprints202302.0328.v1



**Figure 3.** (a) A schematic for a baby fish with a three-dimensional body that freely swims through seawater. (b) A schematic for a grown-up flat fish that sits mostly on the sea bottom. (c) Outstanding fins are denoted as 'af (anal fin)', 'df (dorsal fin)', 'pf (pectoral fin)', and 'tf (tail fin)'. The plane, on which (c) is drawn, is a median plane when disregarding the asymmetry due to the one-sided placement of the two eyes. (d) The left-handed eye pair of olivaceus. (e) The right-handed eye pair of cornutus.

Figure 3c schematically shows several key portions of a grown-up flat fish, where several representative fins are marked such that 'af (anal fin)', 'df (dorsal fin)', 'pf (pectoral fin)', tf (tail fin)'. Notice here that the abdominal portion carries the 'af (anal fin)', while the back portion caries the 'df (dorsal fin)'. Figure 3c is intentionally drawn to carry only a single eye.

While being laid-down near sea bottom, a flat fish would feel that one of its two eyes receives almost no light since that bottom-facing eye almost touches the bottom. The flat fish thus adjusts the placement of the two eyes towards the sunlight. It is because turning itself upside down at regular time intervals is probably more energy-consuming than moving the placement of eyes permanently. Such a rearrangement of eyes takes probably in the early portion of its lifetime (being only a few years). Figure 3d,e show two ways of rearranging its eyes. Figure 3d1,e1 show the top views as seen from the 'df (dorsal fin)' on the backside of a flat fish. From these top views, the eyes of an 'olivaceus' are shifted to the left as depicted on Figure 3d2, whereas the eyes of a 'cornutus' are shifted to the right as depicted on Figure 3e2.

Two different flat fishes of distinct kinds shown on Figure 3d1,e1 are mirror-symmetric across a certain mirror plane (being identical to the median plane) that is parallel to the planes that pierce the fishes along the 'df-af'. Notwithstanding, a mirror-symmetry of a certain flat fish should be determined by examining a mirror-symmetry about a mirror plane that pierces through only a certain single fish. There is hence no mirror-symmetry for a certain lone flat fish with displaced eyes.

Consequently, both kinds of flat fishes illustrated on Figure 3d,e are respectively mirror-asymmetric or chiral, thereby forming an enantiomeric pair. The way chirality is established over a period of a year or so for a flat fish is analogous to the fabrication process of various nano-scale chiral objects [2]. In addition, it remains to further identify other characteristics such as chiral centers, enantiomers, diastereomers, and higher-order enantiomers (HOEs) by working on more details of the schematic Figure 3 [1].

Are there additional features that come with left- and right-handed eye pairs? Yes, there are. A left-handed olivaceus shown on Figure 3d is known to possess a larger mouth than a right-handed cornutus illustrated on Figure 3e. Likewise, the former possesses stronger teeth than the latter. Such distinctions may be compared with the distinctive differences in the arms of left- and right-handed baseball players. The ratio of the total numbers in olivaceus and cornutus may indicate which kind of flat fishes are endowed with better survivability and adaptability to nature. In general, it is known that olivaceus is more available in nature than cornutus. Such a stability difference is also found in many pairs of chiral biopolymers in the sense of enantiomeric excesses [75].

## 5. Temperature Dependence of Chirality

Molecular motors shed light on the relationship between deformation dynamics and energetics. Molecular motors operate by stepping through a repeating cycle of chemical reactions, while undergoing shape changes and executing their own movements. Molecular motors driven either by light or by chemical reactions [76–78], thus being sensitive to temperature changes.

Chemically driven molecular machines are governed possibly by the kinetic asymmetry as a kind of Brownian ratchet. Thermally driven ratchet motions are also reported for magnetic materials [8], where magnetic chirality is allowed only in out-of-equilibrium conditions [79,80]. In this connection, one exemplary motion is either a rotation around a bond or a motion along a track. Instead of uselessly twitching back and forth, unidirectional motions are more useful [40]. Reaction-kinetic asymmetry is key to understanding directionality of kinetic cycles. Likewise, geometric chirality is a key to causing asymmetry in light-driven processes.

 doi:10.20944/preprints202302.0328.v1



Oftentimes, 'unidirectional' and 'chiral' are interchangeably employed in this type of motions [23,81,82]. Such chiral quantum mechanics shares partly analogous formulations with what are discussed here for chiral media. A directed motion on a linear track translates into either clockwise or counterclockwise rotation on a circular track [8]. In terms of light polarization, a linear directed motion corresponds to a linear EM polarization, whereas a circular directed motion corresponds to a circular EM polarization (either clockwise or counterclockwise).

In case with photo-responsive processes, power strokes are involved in driving light-driven molecular machines through absorption of external photon energy [41]. Light excites a molecular machine into a high-energy state, while its relaxation causes large mechanical deformations. The employed photochemical principles in light-driven motions invariably involve temperature dependence and losses in device performance. In case with silicon-based optical materials employed for chemical and biological sensing in the mid-infrared wavelength range, the fundamental vibrational modes of most chemical bonds are of interest [83]. Both molecular motors and molecular switches require largely transient dynamics rather than time-harmonic periodicity for the motion analysis.

In terms of sub-molecular structures, there is enough conformational flexibility in both stator of a molecular motor to prevent excessive distortion of the central bond, which could lead to rapid racemization (becoming achiral) [84]. In case with overcrowded alkene-based molecular motors [41], there are two aspects with respect to chirality: [i] photochemical E-Z (PEZ) isomerization, and [ii] the thermal helix inversion (THI) steps [18]. Resultantly, conformational chirality is likely to arouse unidirectional rotations.

It is instructive to consider a fluid flow through the inside of a solid tube [85]. A laminar Poiseuille flow is normally established when a mean axial flow speed is sufficiently low. If a thin twisted tape is inserted into the inside of a tube, one finds analytically an enhancement in the heat transfer across a tube wall due to the alteration of the flow characters caused by the insertion of a twisted structure.

From the strong dependence on surface states of nanostructures, the stress states of a twisted Omega particles should be more complicated than those of an elliptical particle [57]. Resultantly, an intricate interplay is found between radiation-induced viscous flow, anisotropic strain generation, and capillary stresses [57]. Recently, a variety of twisted meta-atoms are proposed thanks to the modern nanofabrication techniques. Meta-surfaces consisting of such twisted Omega particles on substrates are examined by [6] (pp. 241-263), [13,19,49,86].

Various biochemical activities are influenced by thermal effects, thus resulting in structural changes as can be seen with thermococcuses [87]. Thermophiles (heat-loving organisms) are known to favor relatively high temperature around sixty degrees of Celsius. Optical activity is also exhibited by natural materials [88]. Quartz is a naturally available chiral crystal, for which the temperature dependence of optical chirality is well documented [33,34]. Roughly over the temperature range of $100 \sim 1000^{o} K$, the angle $\theta_{ORD}$ in Equation (4) is known to monotonically increase with temperature.

The twisted Omega meta-atoms depicted on Figure 2a,b are receiving renewed attention [19], partly because their resemblance in structures to a single-strand DNA. DNAs as deformable polymer chains are analyzed under the influence of thermal fluctuations by [89], thereby exhibiting a temperature dependence of phonon dynamics. Most biological matters are soft matters (e.g., in a variety of polymers) [51], thus undergoing conformational changes depending on several factors: the environmental temperature, strains caused by nearby biological matters, embedding fluids, etc. [40].

In ordered crystals, the optical rotatory dispersion (ORD) defined in Equation (4) is also known to be temperature-dependent through the temperature-modulated phonons [33]. Such a temperature-dependent ORD is indicative of the phase transitions occurring within crystallographic structures. Resultantly, the geometric helical property is conducive to the optical chirality for many of crystals.

Optical materials exhibiting phase transitions upon temperature variations are employed for optical switches and modulators. For instance, vanadium dioxides undergo phase transitions between metallic and insulating states due to temperature variations which are caused in turn by externally applied electric potentials [66]. In optical devices based on vanadium dioxides should be

Preprints (www.preprints.org) | NOT PEER-REVIEWED | Posted: 20 February 2023 doi:10.20944/preprints202302.0328.v1



designed by taking the lateral Poisson-ratio effects if typical feature sizes of a device are on the order of optical wavelengths. In this regard, it is stated in [58] that scientists from many different fields still ignore the variability of Poisson's ratio. For the same reason, the twisted Omega particle depicted on Figure 2a would be sensitive to temperature variations.

For a given mass of a meta-atom, its volume varies with temperature variation. More importantly, the Poisson ratio is known to depend on temperature [90]. For instance, crystalline metals exhibit $\nu(T)$ [58,71]. For metals with higher electrical conductivities, the Poisson ratios are also higher in general, thus indicating an increased malleability. Especially for rubbery materials, the Poisson ratio experiences a sharp increase as the temperature is increased across its glass temperature, viz., $\partial\nu(T)/\partial T > 0$ [58]. In contrast, it could happen that $\partial\nu(T)/\partial T < 0$ with some other materials.

There could exist a special temperature $T_\nu$ for a vanishing Poisson ratio, namely, $\nu(T_\nu) = 0$. In this connection, the apparent Poisson ratio of a whole chiral medium should depend on the concentration of the dispersed chiral objects [58]. As a relevant example, a temperature-dependent inversion in the chirality parameter takes place with the homogeneous chiral liquid of ethyl tartrate [35].

In brief,

$$\nu(T_\nu) = 0 . \tag{5}$$

Let us come back to Figure 2a, where an alternating current (AC) of electrons is established along both wire portions and a loop. Especially, the circulatory electric current along a loop induces an effective magnetic field that is parallel to the electric currents along the wire portions [35]. This loop current is alternatively called a 'ring current' [6] (pp. 91-93). The parallel orientation between the electric current and an effective magnetic field is analogous what prevails with chiral (unidirectional) transport anomaly [91,92].

Suppose that increased temperatures lead to differential thermal expansions in different members of a twisted Omega particle depicted on Figure 2b. An assumed co-parallel induced currents in the straight portions shown on Figure 2a could then become non-parallel due to chiral members of the straight portions. In other words, the parallelism would be broken as temperature is varied as illustrated on Figure 2b.

In the study on the electron transport on the crystals of NbAs [91], the magnetization of Weyl semimetals is described approximately by the Lifshitz-Kosevich dependence $\chi/\sinh(\chi)$. Here, $\chi \propto (m^* T)/B$, where $\chi$, $T$, and $B$ are effective mass, temperature, and applied magnetic field. Therefore, smaller effective mass, lower temperature, and larger applied magnetic field are all conducive to a constant limit form $\chi/\sinh(\chi) \to 1$ as $\chi \to 0$. Those chiral anomalies manifest themselves also through strain-induced electron transports [93].

Furthermore, the force between two colloidal particles, each of them carrying one single strand DNA, is theoretically predicted in [94]. Here, a simplest one-dimensional discrete-node model for phonons is adopted with the coupling force between two strands of a double-helix DNA. Temperature dependence can be incorporated into the model of [94] by instituting the temperature dependences of both self-spring and coupling springs. In addition, thermal fluctuations play nontrivial roles in making estimates of stresses and strains in finite-sized nanostructures [42]. In this case, soft maters and hard matters require different approaches based on the distinction between Gibbs ensemble and Helmholtz ensemble [42].

As a kind of typical soft matters, chiral lyotropic chromonic liquid crystals exhibit their helical pitches increasing with temperature [95], whereas an inverse temperature dependence is observed for other kinds of liquid crystals. Such mixed temperature-pitch relations render our expectation on $\{\kappa(T), \beta(T)\}$ extremely confusing for helical structures.

In the meantime, the expansion-contraction scenarios within a solid as illustrated on Figure 2c–f could take place during a short transient process in fabricating nanoparticles by intense ion-beam

Preprints (www.preprints.org) | NOT PEER-REVIEWED | Posted: 20 February 2023 doi:10.20944/preprints202302.0328.v1



irradiations [56], where thermal stresses influence the deformation processes as well. In this regard, viscous and plastic deformations could also take place [57] for thermally grown nanostructures during a fast transient period involving strong ion-beam irradiation fluxes.

Regarding the afore-mentioned chirality-induced spin selection (CISS), both spin polarization (SP) and magnetoresistance ratio (MR) exhibit strong temperature dependence in not only double-stranded DNAs but also alpha-helix oligopeptides [24]. The resulting electric conductivity is found to decrease largely with temperature due to the thermal agitation of phonons (polarons). However, opposite temperature dependences are also observed under other experimental conditions including the substrates and electric contacts. These experimental and modeling results show the importance of including the electron-phonon coupling in a right manner in handling chiral transports through both chiral objects as individuals and chiral media as a composite whole.

There is a possibility of interconversion from a left-handed enantiomer to a right-handed enantiomer or vice versa [96]. Such a thermal (heat-induced) helix inversion (THI) is found from helical diastereoisomers, where chirality undergoes cyclic sign changes according to the pattern $R \to L \to R \to L$. This inversion is associated with the variation in the dihedral angle around a certain bond between two atoms so that it affects the rotational speed of a molecular motor [76]. Such alternating chirality variations can be exploited for realizing afore-mentioned molecular motors and switchable spin-filters [25,41,76]. Magnetic contents of helical structures also affect the helix inversion [23].

**6. Discussions**

The initial introduction of alpha helices came with the notion of a rotation around a helical axis and a translation along a helical axis [75]. *It is noticed in this regard that a homogeneous wire-like thread admits no residue (or residue being zero) when it is deformed into a helix.* In addition to the pitch and helix radius for defining a single homogeneous helix, there are more geometric parameters for defining relationships among constituent (or contributing) helices if sub-helix constituents are looked upon. For such spatially inhomogeneous helices, *residues per helical turn are found to be non-integers in general. For instance, e*ach amino acid corresponds to a helical turn over the angle of $87^o$ in the helix. Therefore, its helix has $360^o/87^o = 4.138$ residues per turn [97] (pp. 95-129). Coiled coils are a set of helices put together so that they are alternatively called 'compound helices' [97] (pp. 95-129).

A desirable side effect of a coiled coil is an increased mechanical rigidity in comparison to its individual constituent helices. As a macromolecule, a coiled coil admits a variety of conformational deformations, thus altering the apparent mechanical strengths. For instance, we find packing-induced superhelical distortions. *Furthermore, alpha-helices are found to be predominantly single-handed between left- and right-handed choices.*

*Afterwards, there appeared numerous investigations into alpha helices.* In the case with alpha-helical peptides [22], the directional transport is called a 'spin filtering'. Upon stretching along the main helical axis of an alpha-helix, an unfolding of a helix takes place to become a beta-strand (or beta-helix), thereby reducing the geometrical chirality [98]. In other words, the pitch gets shortened and the helix radius is enlarged because of the effective Poisson ratio is positive. See Figure 2a,b for comparison.

Such stretching accompanying unfolding could be heat-induced, thus being sensitive to temperature. The stability of an alpha-helix depends on the interactions with an embedding (surrounding) fluid, namely, in the sense of hydrophilicity versus hydrophobicity. Hence, the net chirality exhibited by a single coiled coil poses a challenge of evaluating the attendant EM chirality from the light-matter viewpoint.

Having considered thermal effects on single chiral objects, let us turn to a chiral medium, namely, an ensemble of chiral objects dispersed into an embedding fluid (either liquid or gas). The ensemble of chiral objects may consist of several kinds of enantiomers. For the sake of simplicity in discussion, Figure 3 shows two comparative situations, where blue lightning-rod-like objects and red crescent-like objects stand respectively for left-handed enantiomers (denoted by '-') and right-handed enantiomers (denoted by '+").

Preprints (www.preprints.org) | NOT PEER-REVIEWED | Posted: 20 February 2023 doi:10.20944/preprints202302.0328.v1



Both ensembles on Figure 4a,b consist of blue and red objects, but in different proportions. As a further simplicity, suppose that blue and red objects are more stable respectively in lower and higher temperatures. Therefore, the blue objects undergo thermal helix inversion (THI) with increasing temperature, thereby becoming red objects. As described in the preceding two sections, such THIs between blue and red objects arise from several factors: conformations, thermoelastic properties, electron dynamics, energy contents, etc. In general, both blue and red objects are not necessarily enantiomeric counterparts of each other, for instance, being composed of varying sizes.

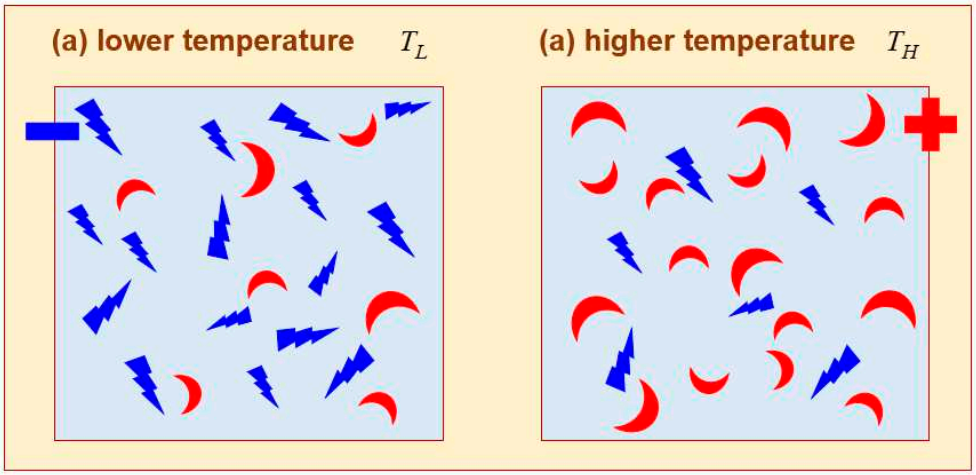


**Figure 4.** Helical inversion temperature (HIT) can be explained by (a) a net left-handed chiral medium and (b) a net right-handed chiral medium.

According to the above simple picture on Figure 4, a helical inversion temperature (HIT) as a transition temperature is defined below.

$$\begin{cases} \kappa(T_\kappa)=0 \\ \beta(T_\beta)=0 \end{cases} : \begin{cases} \kappa(T)<0, & T<T_\kappa \\ \beta(T)<0 & T<T_\beta \end{cases}, \begin{cases} \kappa(T)>0, & T>T_\kappa \\ \beta(T)>0 & T>T_\beta \end{cases}. \tag{6}$$

The converse can be envisaged such that red objects turn into blue objects with increasing temperature. In this converse case, the inequality signs in Equation (6) are reversed of course. In general, $T_\kappa \neq T_\beta$ depending on a particular combination of an embedding medium and dispersed chiral objects. There exists an enantiomeric excess if either $\kappa \neq 0$ or $\beta \neq 0$ [4,35]. The condition either of $\kappa(T_\kappa)=0$ or of $\beta(T_\beta)=0$ is called the 'equal-population condition (EPC)' between left- and right-handed enantiomers.

An example of such transition is discussed in detail for a solution with a variety of polymers as solutes dispersed in various solvents [18]. They considered a polymer consisting of enantiomers of opposite chirality in unequal amount. Such a (nonracemic) chiral polymer could undergo a temperature-dependent transition towards a net achiral (racemic) polymer. That transition temperature is called a compensation (switch) temperature, namely, either of $\{T_\kappa, T_\beta\}$, thus delineating a temperature-dependent helical sense inversion (HSI) or thermally activated helical reversal (TAHR) [18]. In this respect, the solute-solvent interactions should be carefully examined as well.

A mixture of spin-up electrons and spin-down electrons can also be described by Figure 3 [6] (pp. 53-74), whence a one-way spin-dependent channel could be opened for spintronics applications [81]. Recall additionally that there could exist a transition with $\kappa(T_\kappa)=0$ for the Poisson ratio as stated in Equation (5). Due to complex dynamics, $T_\nu \neq T_\kappa$ and $T_\nu \neq T_\beta$ in general.

Helical polymers can be appended with paired structurally different enantiomers. A group of monomers of different species is called a copolymer (for example, terpolymers and quaterpolymers)

[34]. Such conformationally flexible structures could have opposing helical sense preferences. As illustrated on Figure 3, consider a solvent dispersed with two groups of constituent chiral objects [18]. Such a chiral solution exhibits varied helical sense excesses (HSEs) depending on the two factors of the two constituent solutes: [i] relative molar compositions, and [ii] relative chemical energies.

Those composite chiral media yield a new kind of relationship between optical activity (such as ORD) and temperature [18]. In connection with the first item, the enantiomer concentration alluded to by [99] refers to the concentration of, say, a left-handed enantiomer among a mixture of left- and right-handed enantiomers. Therefore, the concentration of the total enantiomers with respect to the embedding medium, not treated by [99], should be taken as an additional factor determining the net chirality.

As regards effective-medium theories (EMTs), we learn that there are no systematic endeavors for an EMT for chiral media. Derivation of such EMTs will be more challenging if there are more than two kinds of constituent chiral objects dispersed in an embedding medium [47]. An extra complication arises from the interactions among the embedding medium and embedded objects if the volume density of embedded objects gets larger.

Helix reversals in polymers are investigated through a random-field Ising model so that the Ising order turns out to correspond to optical activity [18,99]. In this way, optical activity of a helical polymer is evaluated in terms of the magnetization of a random copolymer. Such an evaluation leads to optical activity in terms of enantiomer concentration [99]. We notice particularly that a finite domain size comes into play and hence boundary effects should be taken into consideration [99]. This boundary effect is akin to the solvent-solute interactions. In addition, finite-size effects should be taken into consideration when dealing with DNA-like helical structures as contact potentials [20,21,23]. Mesogenic matters have also been investigated for their diverse roles in both geometric helicity and EM chirality.

Our interest in the interaction between EM waves and chiral media lies in how to make a certain chiral medium straddling about a racemic mixture, namely, switching between a chiral medium in one direction and another chiral medium in opposite direction. By a slight modification of dispersed chiral objects, the chiral medium undergoes a switching between two opposite chiral states. From the viewpoint of optical sensing of chiral media, either $T_\beta$ or $T_\beta$ is termed an 'optical switch temperature (OST)' [18]. The majority rule (referring to a higher concentration between left- and right-handed enantiomers) is hence applied to determine optical activity from a mixture of left- and right-handed enantiomers [18,35].

As sketched on Figure 1, the light-matter interactions between EM waves and a chiral media involve diverse phenomena involving photons, phonons, electrons, etc. Both random thermal fluctuations and imposed thermal gradients will play competing influences on light-matter interactions [8]. In this connection, multiple length and time scales should be taken into consideration [6] (pp. 287-322). The meta-atom with a typical length scale being much shorter than the typical wavelength of EM waves is the fundamental assumption underlying the effective-medium theory [47].

Our discussion on flat fishes shown on Figure 3 gives us some clues as to how to construct chiral metamaterials and chiral meta-surfaces in bio-inspired fashions. There could exist 2D meta-surfaces, where the meta-atoms (building blocks or unit cells) are also 2D. When meta-atoms are made of a single homogeneous medium, the chiral meta-atoms are normally 3D, namely, non-planar [1]. Notice however that planar chiral materials are allowed in stereochemistry where a variety of atoms participate in forming varied materials such as in heterostructures and superlattices [1,71]. Only through effective-medium theory, a meta-surface consisting of 3D meta-atoms appears to be 2D for sufficiently long-wavelength EM fields.

An exact balance as found in racemic mixtures between two kinds of enantiomers are thought to be an exception rather than a rule in nature [4], where one kind of enantiomers are often favored over the other kind of enantiomers. It is said in [1] that an exact symmetry (achirality) is close to death. In this regard, we raise a self-question as to whether the vacuum fluctuations as seen in quantum mechanics have something to do with the nonzero enantiomeric excesses [52] (p. 208). A

possible answer to this self-question transpires to the unachievable state of absolute zero temperature, which in turn corroborates the importance of phonon dynamics and statistical features [6] (pp. 8-20), [8]. Indeed, an achiral mirror-symmetric state is the rarest situation as exemplified by our study on two obliquely colliding EM waves [44].

## 7. Conclusions

We have presented in this review how chiral media are constructed when a chiral medium refers to a liquid dispersed with a random ensemble of chiral objects. We have thus shown the importance of helical structures that incorporate magnetoelectric couplings. Twisted-Omega-particle-like helical structures are examined for their underlying mechanisms. We have examined various typical cross-coupled systems relevant to the interactions between light and chiral media. In various places of those light-matter interactions, the roles played by thermal effects are examined in connection with phonon dynamics which get in interactions with electron transport and magnetic spin transport. We have also identified a possibility of realizing an electromagnetic chiral switching such that the enantiomeric constituents within a chiral medium are differently responsive to temperature variations.

**Author Contributions:** Dr. Lee was organized the overall structure and wrote most of the manuscript. Dr. Lee also prepared materials on electromagnetic chirality. Vaidya and Prof. Dwivedi provided and analyzed literature on thermal effects based on their proficiency in associated phase-transition optical materials and associated optical switching and modulations.

**Funding:** This research was funded by National Research Foundation (NRF) of Republic of Korea under Grant NRF-2018R1D1A1B07045905.

**Data Availability Statement:** There is no underlying data set.

**Conflicts of Interest:** The authors declare no conflict of interest.

## References

1. Adawy, A. Functional Chirality: From Small Molecules to Supramolecular Assemblies. *Symmetry* **2022**, *14*, 292. https://doi.org/10.3390/sym14020292
2. Mun, J., Kim, M., Yang, Y. et al. Electromagnetic chirality: from fundamentals to nontraditional chiroptical phenomena. *Light Sci. Appl.* **2020**, 9, 139. https://doi.org/10.1038/s41377-020-00367-8
3. Wang, X.; He, M.; Ding, F. Chirality-controlled synthesis of single-walled carbon nanotubes-From mechanistic studies toward experimental realization. *Materials Today* **2018**, 21(8), 845-860. https://doi.org/10.1016/j.mattod.2018.06.001
4. Lee, C.; Weber, J.M.; Rodriguez, L.E.; Sheppard, R.Y.; Barge, L.M.; Berger, E.L.; Burton, A.S. Chirality in Organic and Mineral Systems: A Review of Reactivity and Alteration Processes Relevant to Prebiotic Chemistry and Life Detection Missions. *Symmetry* **2022**, *14*, 460. https://doi.org/10.3390/sym14030460
5. Trenti, A.; Borghi, M.; Biasi, S.; Ghulinyan, M.; Ramiro-Manzano, F.; Pucker, G.; Pavesi, L. Thermo-optic coefficient and nonlinear refractive index of silicon oxynitride waveguides. *AIP Advances* **2018**, 8(2), 025311. https://doi.org/10.1063/1.5018016
6. Kamenetskii, E., Chirality, Magnetism and Magnetoelectricity, Separate Phenomena and Joint Effects in Metamaterial Structures. **2021**, Springer.
7. Weißenhofer, M., Nowak, U. Topology dependence of skyrmion Seebeck and skyrmion Nernst effect. *Sci Rep* **2022**, 12, 6801. https://doi.org/10.1038/s41598-022-10550-z
8. Mochizuki, M.; Yu, X.; Seki, S. et al. Thermally driven ratchet motion of a skyrmion microcrystal and topological magnon Hall effect. *Nature Mater* **2014**, 13, 241–246. https://doi.org/10.1038/nmat3862
9. Tabuchi, Y.; Ishino, S.; Ishikawa, T.; Yamazaki, R.; Usami, K.; Nakamura, Y. Hybridizing Ferromagnetic Magnons and Microwave Photons in the Quantum Limit. *Phys. Rev. Lett.* **2014**, 113, 083603. https://doi.org/10.1103/PhysRevLett.113.083603
10. Zograf, G. P.; Petrov, M. I.; Makarov, S. V.; Kivshar, Y. S.All-dielectric thermonanophotonics. *Adv. Opt. Photon.* **2021**, 13, 643-702. https://doi.org/10.1364/AOP.426047
11. Jaggard, D.L., Mickelson, A.R. & Papas, C.H. On electromagnetic waves in chiral media. *Appl. Phys.* **1979**, 18, 211–216. https://doi.org/10.1007/BF00934418
12. Zhao, R.; Koschny, T.; Soukoulis, C. M. Chiral metamaterials: retrieval of the effective parameters with and without substrate. *Opt. Express* **2010**, 18, 14553-14567. https://doi.org/10.1364/OE.18.014553
13. Caloz, C.; Sihvola, A. Electromagnetic Chirality. https://doi.org/10.48550/arXiv.1903.09087

14. Bliokh, K. Y.; Kivshar, Y. S.; Nori, F. Magnetoelectric Effects in Local Light-Matter Interactions. *Phys. Rev. Lett.* **2014**, 113, 033601. https://doi.org/10.1103/PhysRevLett.113.033601
15. Yoo, S.; Park, Q-H. Chiral Light-Matter Interaction in Optical Resonators. *Phys. Rev. Lett.* **2015**, 114, 203003 (2015) https://doi.org/10.1103/PhysRevLett.114.203003
16. Lavigne, G., Kodera, T.; Caloz, C. Metasurface magnetless specular isolator. *Sci Rep* **2022**, 12, 5652. https://doi.org/10.1038/s41598-022-09576-0
17. Kang, H., Lin, T., Xu, X. et al. DNA dynamics and computation based on toehold-free strand displacement. *Nat Commun* **2021**, 12, 4994. https://doi.org/10.1038/s41467-021-25270-7
18. Tang, K.; Green, M. M.; Cheon, K. S.; Selinger, J. V.; Garetz, B. A. Chiral Conflict. The Effect of Temperature on the Helical Sense of a Polymer Controlled by the Competition between Structurally Different Enantiomers: From Dilute Solution to the Lyotropic Liquid Crystal State. *J. Am. Chem. Soc.* **2003**, 125, 7313-7323. https://doi.org/10.1021/ja030065c
19. Sakellari, I.; Yin, X.; Nesterov, M. L.; Terzaki, K.; Xomalis, A.; Farsari, M. 3D Chiral Plasmonic Metamaterials Fabricated by Direct Laser Writing: The Twisted Omega Particle. *Adv. Opt. Mater.* **2017**, 5(16), 1700200. https://doi.org/10.1002/adom.201700200
20. Guo, A.-M.; Díaz, E.; Gaul, C.; Gutierrez, R.; Domínguez-Adame, F.; Cuniberti, G.; Sun, Q.-F. Contact effects in spin transport along double-helical molecules. *Phys. Rev. B* **2014**, 89, 205434. https://doi.org/10.1103/PhysRevB.89.205434
21. Geyer, M.; Gutierrez, R.; Cuniberti, G. Effective Hamiltonian model for helically constrained quantum systems within adiabatic perturbation theory: Application to the chirality-induced spin selectivity (CISS) effect. *J. Chem. Phys.* **2020**, 152, 214105. https://doi.org/10.1063/5.0005181
22. Guo, A.-M.; Sun, Q.-F. Spin-dependent electron transport in protein-like single-helical molecules. *Proc. Natl. Acad. Sci.* **2024**, 111(32), 11658–11662. https://doi.org/10.1073/pnas.1407716111
23. Aiello, C. D.; Abendroth, J. M.; Abbas, M.; et al, A Chirality-Based Quantum Leap. *ACS Nano* **2022**, 16(4), 4989–5035. https://doi.org/10.1021/acsnano.1c01347
24. Das, T. K.; Tassinari, F.; Naaman, R.; Fransson, J. Temperature-Dependent Chiral-Induced Spin Selectivity Effect: Experiments and Theory. *J. Phys. Chem. C* **2022**, 126(6), 3257–3264. https://doi.org/10.1021/acs.jpcc.1c10550
25. Zhu, Q.; Danowski, W.; Mondal, A. K. et al. Multistate Switching of Spin Selectivity in Electron Transport through Light-Driven Molecular Motors. *Adv. Sci.* **2021**, e2101773. https://doi.org/10.1002/advs.202101773
26. Guida, G.; Maystre, D.; Tayeb, G.; Vincent, P. Mean-field theory of two-dimensional metallic photonic crystals. *J. Opt. Soc. Am. B* **1998**, 15, 2308-2315. https://doi.org/10.1364/JOSAB.15.002308
27. Mi, G.; Van, M. Characteristics of surface plasmon polaritons at a chiral–metal interface. *Opt. Lett.* **2014**, 39, 2028-2031. https://doi.org/10.1364/OL.39.002028
28. Lee, H.-I.; Gaul, C. **Sign flips, crossovers, and spatial inversions in surface plasmon resonance across a chiral-metal interface. *Opt. Lett.* 2023, 48(4).** https://doi.org/10.1364/OL.484329
29. Margineda, J.; Molina-Cuberos, G. J.; Núñez, M. J.; García-Collado, A. J.; Martín, E. Electromagnetic Characterization of Chiral Media", Solutions and Applications of Scattering, Propagation, Radiation and Emission of Electromagnetic Waves, Edited by Ahmed Kishk, *IntechOpen* **2012**. https://doi.org/10.5772/51539
30. Yoo, S.; Park, Q-H. Enhancement of Chiroptical Signals by Circular Differential Mie Scattering of Nanoparticles. *Sci. Rep.* **2015,** 5, 14463. https://doi.org/10.1038/srep14463
31. Cho, K. Dispersion Relation in Chiral Media: Credibility of Drude-Born-Fedorov equations. https://doi.org/10.48550/arXiv.1501.01078
32. Freire-Fernández, F., Cuerda, J., Daskalakis, K.S. et al. Magnetic on–off switching of a plasmonic laser. *Nat. Photon.* **2022, 16,** 27–32. https://doi.org/10.1038/s41566-021-00922-8
33. Yogev-Einot, D.; Avnir, D. The temperature-dependent optical activity of quartz: from Le Châtelier to chirality measures. *Tetrahedron: Asymmetry* **2006**, 17(19), 2723-2725. https://doi.org/10.1016/j.tetasy.2006.10.004
34. Lowry, T. M. Optical Rotatory Power; Dover Publications, New York, **1964**.
35. Condon, E. U. Theories of Optical Rotatory Power. *Rev. Mod. Phys.* **1937**, 9, 432. https://doi.org/10.1103/RevModPhys.9.432
36. Droulias, S.; L. Bougas, L. Chiral sensing with achiral anisotropic metasurfaces. *Phys. Rev. B* **2021**, *104, 075412.* https://doi.org/10.1103/PhysRevB.104.075412
37. Sikes, D.E.; Yavuz, D. D. Negative refraction with low absorption using Raman transitions with magnetoelectric coupling. *Phys. Rev. A* **2010**, 82, 011806(R). https://doi.org/10.1103/PhysRevA.82.011806
38. Kuzmin, D. A.; Bychkov, I. V.; Shavrov, V. G.; Temnov, V. V., Lee, H.-I.; Mok, J. Plasmonically induced magnetic field in graphene-coated nanowires. *Opt. Lett.* **2016**, 41, 396-399. https://doi.org/10.1364/OL.41.000396
39. Lee, H-I. Spin–Orbital Coupling and Conservation Laws in Electromagnetic Waves Propagating through Chiral Media. *Optics* **2023**, 4(1), 100-131. https://doi.org/10.3390/opt4010008

40. Ha, T. Probing Nature's Nanomachines One Molecule at a Time. *Biophysical J.* **2016**, 110(5), 1004-1007.:https://doi.org/10.1016/j.bpj.2016.02.009
41. Pooler, D. R, S.; Lubbe, A. S.; Crespi, S.; Feringa, B. L. Designing light-driven rotary molecular motors. *Chem Sci.* **2021**, 12,14964-14986. https://doi.org/10.1039/d1sc04781g
42. Bellino, L.; Florio, G.; Stefano Giordano, Giuseppe Puglisi, On the competition between interface energy and temperature in phase transition phenomena. *Applications in Engineering Science* **2020**, 2, 100009. https://doi.org/10.1016/j.apples.2020.100009
43. Barba, I.; Cabeceira, A.C.L.; García-Collado, A.J.; Molina-Cuberos, G. J.; Margineda, J.; Represa, J. Quasi-planar Chiral Materials for Microwave Frequencies. Electromagnetic Waves Propagation in Complex Matter, Edited by Ahmed Kishk, *IntechOpen* **2011**, Chap. 4, 97-116. https://doi.org/10.5772/16999
44. Lee, H.-I. Anti-Symmetric Medium Chirality Leading to Symmetric Field Helicity in Response to a Pair of Circularly Polarized Plane Waves in Counter-Propagating Configuration. *Symmetry* **2022**, 14, 1895. https://doi.org/10.3390/sym14091895
45. Lee, H.-I. Spin–Orbital Coupling and Conservation Laws in Electromagnetic Waves Propagating through Chiral Media. *Optics* **2023**, *4*, 100-131. https://doi.org/10.3390/opt4010008
46. Kim, S.; Kim, K. "Excitation of surface waves on the interfaces of general bi-isotropic media. *Opt. Express* **2016**, 24, 15882-15896. https://doi.org/10.1364/OE.24.015882
47. Markel, V. A. Maxwell Garnett approximation in random media: tutorial. *J. Opt. Soc. Am. A* **2022**, 39, 535-544. https://doi.org/10.1364/JOSAA.450850
48. Ioannis G. Stratis, Athanasios N. Yannacopoulos, "Electromagnetic fields in linear and nonlinear chiral media: a time-domain analysis", *Abstract and Applied Analysis* **2004**, 583247. https://doi.org/10.1155/S1085337504306287
49. Lekner, J. Invariants of electromagnetic beams. *J. Opt. A: Pure Appl. Opt.* **2004**, 6, 204. https://doi.org/10.1088/1464-4258/6/2/008
50. Bohren, C.F.; Huffman, D.R. Absorption and Scattering of Light by Small Particles; Wiley: New York, NY, USA, **1983**.
51. Lakhtakia, A.; Varadan, V. V.; Varadan, V. K. Field equations, Huygens's principle, integral equations, and theorems for radiation and scattering of electromagnetic waves in isotropic chiral media. *J. Opt. Soc. Am. A* **1988**, 5, 175-184. https://doi.org/10.1364/JOSAA.5.000175
52. Barron, L. D. Molecular Light Scattering and Optical Activity, 2nd ed.; Cambridge Univ. Press: Cambridge, U.K., **2004**.
53. Yin, R.; Li, Y. Zero-viscosity-capillarity limit to the planar rarefaction wave for the 2D compressible Navier–Stokes–Korteweg equations. *Nonlinear Analysis: Real World Applications* **2022**, 68, 103685. https://doi.org/10.1016/j.nonrwa.2022.103685
54. Chen, Z.; He, L.; Zhao, H. Global smooth solutions to the nonisothermal compressible fluid models of Korteweg type with large initial data. *Z. Angew. Math. Phys.* **2017**, 68, 79. https://doi.org/10.1007/s00033-017-0822-8
55. Dunn, J.E.; Serrin, J. On the Thermodynamics of Interstitial Working. Retrieved from the University of Minnesota Digital Conservancy, **1983**. https://hdl.handle.net/11299/4431
56. van Dillen, T.; Polman, A.; Onck, P. R.; van der Giessen, E. Anisotropic plastic deformation by viscous flow in ion tracks. *Phys. Rev. B* **2005**, 71, 024103. https://doi.org/10.1103/PhysRevB.71.024103
57. van Dillen, T.; van der Giessen, E.; Onck, P. R.; Polman, A. Size-dependent ion-beam-induced anisotropic plastic deformation at the nanoscale by nonhydrostatic capillary stresses. *Phys. Rev. B* **2006**, 74, 132103. https://doi.org/10.1103/PhysRevB.74.132103
58. Greaves, G., Greer, A., Lakes, R. et al. Poisson's ratio and modern materials. *Nature Mater* **2011**, 10, 823–837. https://doi.org/10.1038/nmat3134
59. Wojciechowski, K.W. Remarks on "Poisson Ratio beyond the Limits of the Elasticity Theory". *J. Phys. Soc. Jpn.* **2003**, *72*, 1819–1820. https://doi.org/10.1143/jpsj.72.1819
60. Prall, D.; Lakes, R. S. Properties of a chiral honeycomb with a Poisson's ratio of -1. *Int. J. Mech. Sci.* **1997**, 39(3), 305-314. https://doi.org/10.1016/S0020-7403(96)00025-2
61. Wu, W.; Tao, Y.; Xia, Y.; Chen, J.; Lei, H.; Sun, L.; Fang, D. Mechanical properties of hierarchical anti-tetrachiral metastructures. *Extreme Mech. Lett.* **2017**, 16, 18-32. https://doi.org/10.1016/j.eml.2017.08.004
62. Eidini, M. Zigzag-base folded sheet cellular mechanical metamaterials. *Extreme Mech. Lett.* **2016**, 6, 96–102. https://doi.org/10.1016/j.eml.2015.12.006
63. Dörfler, P. K. On the High-partial-load Pulsation in Francis Turbines. *Int. J. Fluid Mach. Syst.* **2019**, 12(3), 200-216. http://doi.org/10.5293/IJFMS.2019.12.3.200
64. Anderson, N.; Hartschuh, A.; Novotny, L. Chirality changes in carbon nanotubes studied with near-field Raman spectroscopy. *Nano Letter* **2007**, 7, 577-582. https://doi.org/10.1021/nl0622496
65. Lee, H.-I. Near-field analysis of electromagnetic chirality in the Mie scattering by a dielectric sphere. *Opt. Continuum* **2022**, 1, 1918-1931. https://doi.org/10.1364/OPTCON.465265

66. Chauhan, D.; Sbeah, Z.; Adhikari, R.; Thakur, M. S.; Chang, S. H.; Dwivedi, R. P. Theoretical analysis of $VO_2$ filled double rectangular cavity-based coupled resonators for plasmonic active switch/modulator and band pass filter applications. *Optical Materials* **2022**, 125, 112078. https://doi.org/10.1016/j.optmat.2022.112078
67. Jacob, K. T.; Shekhar, C.; Vinay, M. Thermodynamic Properties of Niobium Oxides. *J. Chem. Eng. Data* **2010**, 55, 4854–4863. https://doi.org/10.1021/je1004609
68. Stihler, C.; Jauregui, C.; Tünnermann, A.; Limpert, J. Modal energy transfer by thermally induced refractive index gratings in Yb-doped fibers. *Light Sci. Appl.* **2018**, 7, 59. https://doi.org/10.1038/s41377-018-0061-6
69. Anderson, I. A.; Gisby, T. A.; McKay, T. G.; O'Brien, B. M.; Calius, E. P. Multi-functional dielectric elastomer artificial muscles for soft and smart machines. *J. Appl. Phys.* **2012**, 112, 041101. https://doi.org/10.1063/1.4740023
70. Carpi, A. M.; Giorgio, S.; De Rossi, D. Helical dielectric elastomer actuators. *Smart Mater. Struct.* **2005**, 14(6), 1210. https://doi.org/10.1088/0964-1726/14/6/014
71. Kastuar, S. M.; Ekuma, C. E.; Liu, Z. L. Efficient prediction of temperature-dependent elastic and mechanical properties of 2D materials. *Sci Rep* **2022**, 12, 3776. https://doi.org/10.1038/s41598-022-07819-8
72. Carenza, L. N.; Gonnella, G.; Marenduzzo, D.; Negro, G. Rotation and propulsion in 3D active chiral droplets. *Proc. Natl. Acad. Sci.* **2019**, 116(44), 22065-22070. https://doi.org/10.1073/pnas.191090911
73. Johnston, Jr, W. D.; Kaminow, I.P. Temperature Dependence of Raman and Rayleigh Scattering in LiNbO3 and LiTaO3. *Phys. Rev.* **1969**, 178, 1528. https://doi.org/10.1103/PhysRev.178.1528.2
74. These two kinds of fishes have already been documented in the first Korean encyclopedia 'Jibong-Yooseol'. This encyclopedia was started by Korean enlightenment-scientist in the year of 1614. The pseudonym (i.e., pen name) 'Jibong' stands for the author, whose real name is 'Soo-Gwang Lee'. His two sons completed this encyclopedia in 1634. Meanwhile, 'Yooseol' means 'encyclopedia'. This encyclopedia was written in Chinese as usual in that era so that only several Korean translations are available at this moment. Koreans eat these flat fishes either raw or cooked.
75. *Pauling, L.; Corey, R. B.; Branson, H. R. (April 1951). "The structure of proteins; two hydrogen-bonded helical configurations of the polypeptide chain. Proc. Natl. Acad. Sci* ***1951****, 37 (4), 205–11.* https://doi.org/10.1073/pnas.37.4.205
76. Wen, J.; Zhu, M.; González, L. Solvation Effects on the Thermal Helix Inversion of Molecular Motors from QM/MM Calculations. *Chemistry* **2022**, 4, 185-195. https://doi.org/10.3390/chemistry4010016
77. Goldup, S.; Aprahamian, I. Off Detailed Balance: Non-Equilibrium Steady States in Catalysis, Molecular Motors and Supramolecular Materials. *ChemRxiv*, https://doi.org/10.26434/chemrxiv-2022-49s4d-v2
78. Astumian R. D.; Mukherjee S.; Warshel, A. The Physics and Physical Chemistry of Molecular Machines Chemphyschem : a European journal of chemical physics and physical chemistry **2016**, 17(12), 1719-1741. https://doi.org/10.1002/cphc.201600184
79. Astumian, R.D. Kinetic asymmetry allows macromolecular catalysts to drive an information ratchet. *Nat Commun* **2019**, 10, 3837. https://doi.org/10.1038/s41467-019-11402-7
80. Pezzato, C.; Cheng, C.; Stoddart, J. F.; Astumian, R. D. Mastering the non-equilibrium assembly and operation of molecular machines. *Chem. Soc. Rev.* **2017**, 46, 5491-5507. https://doi.org/10.1039/C7CS00068E
81. Lodahl, P.; Mahmoodian, S.; Stobbe, S.; Rauschenbeutel, A.; Schneeweiss, P.; Volz, J.; Pichler, H.; Zoller, P. Chiral quantum optics. *Nature* **2017**, 541,473–480. https://doi.org/10.1038/nature21037
82. James, D. F. V. Quantum kinematics in terms of observable quantities and the chirality of entangled two-qubit states. *J. Opt. Soc. Am. A* **2022**, 39, C86-C97. https://doi.org/10.1364/JOSAA.471796
83. Sinclair, G. F.; Tyler, N. A.; Sahin, D.; Barreto, J.; Thompson, M. G. Temperature Dependence of the Kerr Nonlinearity and Two-Photon Absorption in a Silicon Waveguide at 1.55 μm. *Phys. Rev. Applied* **2019**, 11, 044084. https://doi.org/10.1103/PhysRevApplied.11.044084
84. García-López, V.; Liu, D.; Tour, J. M. Light-Activated Organic Molecular Motors and Their Applications. *Chem. Rev.* **2020**, 120(1), 79–124. https://doi.org/10.1021/acs.chemrev.9b00221
85. Sundar, L.S., Singh, M.K., Pereira, A.M. et al. Augmentation of Heat Transfer of High Prandtl Number $Fe_3O_4$/vacuum pump oil nanofluids flow in a tube with twisted tape inserts in laminar flow. *Heat Mass Transfer* **2020,** 56, 3111–3125 (2020). https://doi.org/10.1007/s00231-020-02913-x
86. Sheng, L.; Zhou, X.; Zhong, Y.; Zhang, X.; Chen, Y.; Zhang, Z.; Chen, H.; Lin, X. Exotic Photonic Spin Hall Effect from a Chiral Interface", Laser Photonics Rev. **2022**, 2200534. https://doi.org/10.1002/lpor.202200534
87. Rodriguez, A. C.; Park, H. W.; Mao, C.; Beese, L. S. Crystal structure of a pol alpha family DNA polymerase from the hyperthermophilic archaeon thermococcus sp. 9 degrees N-7. *J. Mol Biol.* **2000**, 299, 471-487. https://doi.org/10.1006/jmbi.2000.3728
88. Lakhtakia, A. Selected Papers on Natural Optical Activity, **1990**, SPIE Press.
89. Schellman, J. A. Flexibility of DNA. *Biopolymers* **1974**, 13(1), 217-226. https://doi.org/10.1002/bip.1974.360130115

90. Carneiro, V.H.; Puga, H. Temperature Variability of Poisson's Ratio and Its Influence on the Complex Modulus Determined by Dynamic Mechanical Analysis. *Technologies* **2018**, *6*, 81. https://doi.org/10.3390/technologies6030081
91. Naumann, M.; Arnold, F.; Medvecka, Z.; Wu, S.-C.; Süss, V.; Schmidt, M.; Yan, B.; Huber, N.; Worch, L.; Wilde, M. A.; Felser, C.; Sun, Y.; Hassinger, E. Weyl Nodes Close to the Fermi Energy in NbAs. *Physica Status Solidi b* **2022**, 259(5), 2100165 . https://doi.org/10.1002/pssb.202100165
92. Arnold, F.; Naumann, M.; Wu, S.-C.; Sun, Y.; Schmidt, M.; Borrmann, H.; Felser, C.; Yan, B.; Hassinger, E., Chiral Weyl Pockets and Fermi Surface Topology of the Weyl Semimetal TaAs. *Phys. Rev. Lett.* **2016**, 117, 146401, 1-5. https://doi.org/10.1103/PhysRevLett.117.146401
93. Naumann, M.; Mokhtari, P.; Medvecka, Z.; Arnold, F.; Pillaca, M.; Flipo, S.; Sun, D.; Rosner, H.; Leithe-Jasper, A.; Gille, P., Baenitz, M.; Hassinger, E. Fermi surface of the skutterudite $CoSb_3$: Quantum oscillations and band-structure calculations. *Phys. Rev. B* **2021**, 103(8), 085133 (2021) https://doi.org/10.1103/PhysRevB.103.085133
94. de Gennes, P.-G. Maximum Pull Out Force on DNA Hybrids. *C. R. Acad. Sci. Series IV Phys.* **2001**, 2, 1505−1508. https://doi.org/10.1016/S1296-2147(01)01287-2
95. Ogolla, T.; Paley, R. S.; Collings, P. J. Temperature dependence of the pitch in chiral lyotropic chromonic liquid crystals. *Soft Matter* **2019**, 15, 109-115. https://doi.org/10.1039/C8SM02091D
96. Cass, M. E.; Hii, K. K.; Rzepa, H. S. Mechanisms That Interchange Axial and Equatorial Atoms in Fluxional Processes: Illustration of the Berry Pseudorotation, the Turnstile, and the Lever Mechanisms via Animation of Transition State Normal Vibrational Modes. *J. Chem. Educ.* **2006**, 83, 2, 336. https://doi.org/10.1021/ed083p336.2
97. Parry, D. A. D.; Squire, J. M. Fibrous Proteins: Structures and Mechanisms, Subcellular Biochemistry 82, Springer International Publishing AG **2017**. https://doi.org/10.1007/978-3-319-49674-0_4
98. Alizadeh-Rahrovi, J.; Ebrahim-Habibi, A. Unfolding of an alpha-helical peptide exposed to high temperature: suggesting a critical residue in the process. *Struct Chem* **2022**. https://doi.org/10.1007/s11224-022-02038-3
99. Selinger, J. V.; Selinger, R. L. B. Theory of Chiral Order in Random Copolymers. *Phys. Rev. Lett.* **1996**, 76, 58. https://doi.org/10.1103/PhysRevLett.76.58